Available online at www.sciencedirect.com
SCIENCE DIRECT®
Experimental Thermal and Fluid Science xxx (2006) xxx–xxx
Experimental Thermal and Fluid Science
www.elsevier.com/locate/etfs

Planar temperature imaging using thermally assisted laser induced fluorescence of OH in a methane–air flame

C. Copeland [a], J. Friedman [b], M. Renksizbulut [a,*]

[a] University of Waterloo, Mechanical Engineering Department, Waterloo, Ont., Canada N2L 3G1
[b] Ryerson University, Mechanical Engineering Department, Toronto, Ont., Canada M5B 2K3

Received 11 April 2006; accepted 12 April 2006

Abstract

The present study seeks to demonstrate the use of vibrational thermally assisted laser induced fluorescence of the hydroxyl radical to obtain planar temperature measurements. This technique utilizes a simple two-level vibrational model to describe the relationship between the population ratio of excited states and temperature. The quenching to vibrational transfer ratio between the excited states was used as a calibration parameter to fit the thermally assisted fluorescence measurements to known temperature data. The measurements presented here are from a premixed methane–air flame. A rectangular shaped burner allowed for calibration and comparison of the thermally assisted temperature results with sodium line reversal data available in literature. Excellent agreement between the two approaches was achieved for three different equivalence ratios. A single calibration was sufficient for the range of conditions tested in the present work. Two detection schemes were also tested, the first using the (0–0) and (1–0) vibrational bands and the second substituting the (0–1) fluorescence in place of the (0–0) band. The weakness of the fluorescence signal from the (0–1) band was very restrictive to temperature imaging with the current setup. Overall, the applicability of the thermally assisted technique to temperature imaging was positively demonstrated from this work.

Keywords: Combustion; Laser diagnostics; Planar laser-induced fluorescence; Planar thermometry; Temperature measurement; OH fluorescence

1. Introduction

The modern combustion experimentalist has come to increasingly rely on laser based diagnostic tools that were once considered state-of-the-art. These optical measurement methods offer the means for accurate, non-intrusive measurements with excellent temporal and spatial resolution. Practical combustion systems are harsh environments with turbulent quantities that vary with space and time, and as such present many unique challenges to the researcher. Analyzing this complex interplay of chemical and physical mechanisms often requires simultaneous measurement of two or more of the basic quantities: temperature, pressure, species concentration, and flow velocity. This requirement, as well as limitations of cost and experimental complexity, must all be considered in selecting a laser diagnostic approach suitable for a specific application. A large body of research has accumulated to date covering the various laser diagnostic approaches and their applicability in measuring these fundamental quantities under different conditions.

Temperature plays a critical role in understanding a combustion process. It is intimately tied to the chemical kinetics, pollution and soot formation, energy release rates, and overall combustion efficiency. Accurate temperature measurements are necessary for fundamental research in validating theoretical and numerical models, as well as for applied combustion diagnostics. Thermocouple probes have been utilized for temperature measurements for many years, and their low cost and ease of use continue to make

* Corresponding author. Tel.: +1 519 888 4567x3977; fax: +1 519 885 5862.
E-mail address: metin@uwaterloo.ca (M. Renksizbulut).

0894-1777/$ - see front matter © 2006 Elsevier Inc. All rights reserved.
doi:10.1016/j.expthermflusci.2006.04.005

Nomenclature

A_{nm}	spontaneous emission rate constant from energy state n to m
ΔE_{nm}	energy difference between energy states n and m
F_{nm}	fluorescence collected from the transition between states n and m
k	Boltzmann constant (1.38×10^{-23} J/K)
n	number of data points
N_n	population density of energy level n
Q	quenching rate constant
T	temperature
v	vibrational quantum number
V_f	laser focal volume
V_{nm}	vibrational transfer rate constant from energy state n to m

Greek symbols

ε	light collection efficiency
η	optical quantum efficiency
ϕ	mixture equivalence ratio
Ω	solid angle of collection

Acronyms

SLR	sodium line reversal
SNR	signal to noise ratio
THAF	thermally assisted fluorescence
VET	vibrational energy transfer
RMS	root mean square

them indispensable tools to the experimentalist. However, thermocouples suffer from a range of inaccuracies inherent to their intrusive nature. Placing a foreign object into a reactive flow serves to introduce thermal mass and flow perturbations, thus disturbing the chemistry and physics dictating the very property being measured. In contrast, laser based methods not only provide a non-intrusive means to measure temperature, but also offer a number of other advantages. Depending on the individual technique, laser techniques offer the potential for single shot, two-dimensional measurements capable of resolving turbulent information. Most attractively, if the temperature measurement can be made in conjunction with a second quantity such as species concentration from a single laser pulse, this is of considerable interest for improved turbulence modeling.

A number of laser techniques have been developed that are applicable to temperature measurements. They are generally divided into two major groups, depending on whether the resulting signal is coherent or incoherent. Coherent techniques such as degenerate four wave mixing and coherent anti-stokes Raman spectroscopy (CARS) produce superior signal to noise ratios but tend to be quite experimentally complex. Incoherent approaches such as Rayleigh scattering, linear Raman scattering, and laser induced fluorescence (LIF) produce a scattered signal from the interaction of the laser source with the reaction zone constituents. Despite the greater susceptibility to background noise, the advantages of incoherent techniques make them the method of choice in many applications. They are comparatively simple to understand and operate and are easily adapted to two-dimensional imaging with a laser sheet and high-speed camera. Rayleigh scattering produces an elastically scattered signal that is proportional to total number density, which can then be related to temperature through the ideal gas assumption. Two-dimensional Rayleigh temperature imaging has been demonstrated in a number of applications but is limited to low particulate environments where Mie scattering will not cause interference concerns [1,2]. Linear Raman scattering has also been applied to planar temperature imaging but presents unique difficulties due to much lower signal levels [3]. Combining Rayleigh and Raman images to produce a single averaged temperature map has been shown to produce good agreement with numerical results [4].

Arguably the most successful incoherent technique, laser induced fluorescence (LIF) has emerged as an important tool for the combustion researcher. The ample fluorescence signal allows for the detection of minor species and volatile radicals such as OH present in low concentrations. Thus, planar imaging of the OH radical concentration is quite common to experimental combustion research as it serves as a key reaction zone marker and produces sufficient signal for single shot planar measurements useful in turbulent studies [5]. In addition to temperature measurement to be detailed shortly, planar laser-induced fluorescence (PLIF) has also been used for measurements of velocity and pressure fields, indicating its versatility [6].

Thermometry using PLIF has been demonstrated in a number of combustion applications with a variety of seeded and naturally occurring species, mainly using the two-line approach [7–10,30]. In order to capture a temperature image in a non-steady flame using this method, two lines are pumped using two laser sources with pulses separated in time by an amount less than the smallest turbulent fluctuations. The ratio of the two resulting fluorescence images is then used to produce the final temperature map. Two-line LIF thermometry has the advantage of limiting the influence of variations in fluorescence yield by selecting the laser pump lines such that the indicator species is excited to the same upper energy level by each laser pulse. However, this is not always feasible as the selection of the excitation lines is mainly governed by the energy separation required for adequate temperature sensitivity and the transitions available for the particular species being targeted [7]. In addition, the advantages of planar two-line thermometry do come at

the price of significant experimental complexity. The use of two laser sources requires two cameras gated to each laser pulse to capture the fluorescence signals, each of which must be calibrated for differences in laser pulse energy and camera response. Therefore, with the requirement of two laser sources, two intensified cameras, and a system to monitor laser sheet intensity, this technique can become a costly and elaborate addition to a combustion research project.

In comparison to two-line fluorescence, thermometry using thermally assisted fluorescence (THAF) is simpler but has received less attention due to its reliance on upward collisional energy transfer. Both two-line and THAF thermometry measure the excited state fluorescence intensities, but the former relates the fluorescence to temperature through a Boltzmann distribution of ground state populations while the latter relates the distribution of excited quantum states to temperature. THAF uses a single laser source to populate an excited state, and collisional transfer then distributes that population among other excited energy states. For molecular THAF, this means a distribution between rotational states within the vibrational level and among other vibrational levels within the electronic excited state. Following redistribution, the spontaneous emission from two or more of these energy levels can be related to temperature.

A number of authors have used THAF for point temperature measurements with promising results [11–19]. Zizak and Winefordner [11] and Elder et al. [12] measured temperatures from the thermally assisted atomic fluorescence of seeded thallium. Similarly, Joklik et al. [13] reported temperature measurements using fluorescence from seeded gallium atoms. The work of these authors demonstrated that a partial Boltzmann distribution is generally achieved in collisionally excited energy levels that are removed from the laser populated state. This yields a simple Boltzmann temperature relation that holds true, providing the rates of vibrational transfer between these states are much higher than the quenching transfer out of them. More commonly, thermally assisted molecular fluorescence of the hydroxyl radical (OH) has been selected as a temperature indicator. OH has several advantages that make it a popular choice. Since it is one of the more plentiful minor species and plays a large role in the combustion chain reactions of hydrocarbon fuels, it has been studied extensively. This means that first, OH spectroscopic information is readily available, and second that OH–THAF would be an ideal extension to an existing experimental setup, permitting simultaneous OH concentration and temperature measurements. These observations, and the troublesome nature of seeded flows, make the naturally occurring OH radical a common selection for fluorescence experiments.

Chan and Daily [14], and Zizak et al. [15] used the redistribution of OH radicals among rotational energy states to furnish a temperature dependent fluorescence signal. Similar to atomic THAF, temperature was derived based on a partial Boltzmann distribution of collisionally populated rotational states. A simpler approach using the fluorescence from OH vibrational populations was first proposed by Crosley and Smith [16]. Instead of resolving rotational transitions, their analytical treatment generated a two-level model relating temperature to the population ratio of the first two vibrational states within the $A^2\Sigma$ excited manifold. However, since this model relies on the fluorescence from a laser-populated state, this introduces the need to account for the non-Boltzmann character through a collisional energy term. They calculated this term using vibrational and quenching cross sections of the various combustion constituents taken from low pressure, room-temperature experiments. Despite promising results, this work highlighted a weakness in accurately accounting for the quenching effects by analytical means.

Noting the simplicity of the method and the applicability to planar imaging, Dyer and Crosley [17] re-examined the use of the OH vibrational model proposed by Crosley and Smith [16]. This work sought to develop a method to accurately account for collisional effects that posed the earlier difficulty. First, they attempted to measure the collisional terms through vibrational down transfer experiments but found that this produced unrealistic temperatures. However, by accounting for the collisional effects through calibration with measured thermocouple values, excellent agreement was achieved. Despite their original intent, the authors did not feel that the method was sufficiently grounded to proceed with temperature imaging. Therefore, to further this work, Joklik [18] published a comprehensive examination of the applicability of OH vibrational THAF to a variety of combustion conditions. Using three different fuel types and by varying the equivalence ratio of each, this produced a flame temperature range between 1700 K and 2700 K. Collisional transfer rates were modeled numerically as well as calculated through a calibration at sodium line reversal temperatures. The detailed nature of this study gave legitimacy to the OH vibrational THAF method and established the basis for the current work.

Although some have commented on the possibility of extending THAF to planar temperature imaging, all the work outlined thus far has been single-point temperature measurements. It would appear that the only exception to this is the work of Burket et al. [19] who successfully used vibrational THAF of formaldehyde to obtain low temperature images of a self-igniting, *n*-decane droplet. Considering the applicability to two-dimensional imaging as demonstrated chiefly by the work of Joklik [18] and the experimental simplicity of using a single laser source, there is certainly sufficient motivation in seeking to develop the thermally assisted method beyond point temperature measurements. With this in mind, the current research aim was to demonstrate the feasibility of using OH vibrational THAF to obtain two-dimensional temperature data from a premixed methane–air flame.

2. Theory and background

The basic premise of any laser-based measurement strategy is to formulate a set of equations that model the behavior of an atom or molecule under laser excitation, and to relate this behavior to the quantity being measured. Therefore, each theoretical model will be tailored to suit the particular application of laser induced fluorescence. While each approach is unique, there are also similarities between the different LIF theoretical treatments. Most models employ a steady state assumption, which assumes that the population of a given level can be determined by balancing the rates of transfer in and out of that level. This results in an equation that relates the observed fluorescence to the undisturbed population distribution for temperature or number density. Thermally assisted fluorescence is distinctive in that it does not rely on the temperature dependency of the ground state distribution but uses the collisional dynamics of a laser excited atom or molecule to obtain the temperature measurements. The simplest model is the two-level vibrational model introduced by Crosley and Smith [16]. Coincidentally, it is also the approach that is most applicable to planar measurements. Joklik [18] demonstrated this by using bandpass filters to optically integrate the collected vibrational thermally assisted fluorescence. Therefore, this model was used in this work to relate the observed fluorescence intensities to temperature.

Vibrational thermally-assisted laser induced fluorescence is most plainly explained as a three-step process. First, the OH molecules are excited from the $v'' = 0$ vibrational level of the ground $X^2\Pi$ state to the $v' = 0$ vibrational level of the $A^2\Sigma$ state by tuning the laser to a selected rotational transition. Secondly, vibrational energy transfer (VET) promotes a fraction of the excited population from the $v' = 0$ to the $v' = 1$ level. Lastly, the spontaneous emission from each of these levels is simultaneously recorded and related to temperature. These three steps are shown in Fig. 1.

To formulate the temperature relation following the treatment of Crosley and Smith [16], a steady state rate balance is applied to the $v' = 1$ vibrational level as shown in Fig. 2:

$$V_{01}N_0 = (V_{10} + A_1 + Q_1)N_1 \tag{1}$$

where V_{01} is the upward vibrational transfer rate and V_{10} is the downward vibrational transfer rate between the two excited vibrational levels. Any other energy loss is contained in the rate Q_1 which represents the rate of quenching to all other levels. A_1 and A_0 are the rates of spontaneous emission, and N_1 and N_0 are the populations at $v' = 1$ and $v' = 0$ respectively. Upward vibrational transfer can then be related to the downward vibrational transfer through detailed balancing:

$$V_{01} = V_{10}\exp(-\Delta E_{10}/kT) \tag{2}$$

where k is the Boltzmann constant, T the absolute temperature, and ΔE_{10} the energy difference between excited

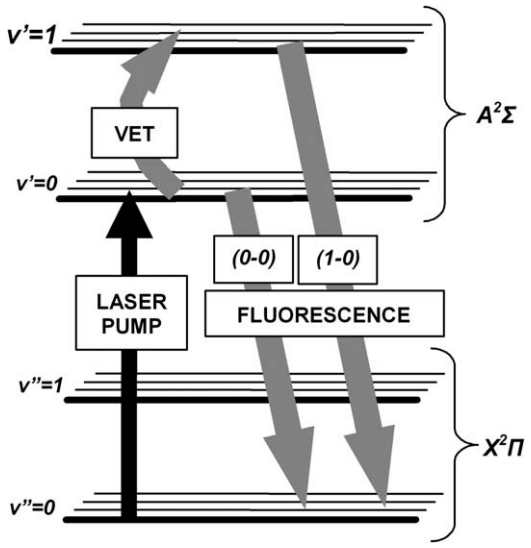

Fig. 1. Thermally assisted fluorescence process.

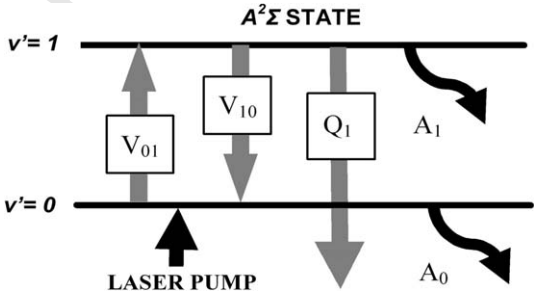

Fig. 2. Rate balance applied to the $v' = 1$ vibrational level.

vibrational levels. If A_1 is taken as orders of magnitude smaller than V and Q in Eq. (1), it can effectively be ignored. Substituting Eq. (2) into (1) then yields:

$$T = \frac{-\Delta E_{10}/k}{\ln[(1 + Q_1/V_{10}) \cdot (N_1/N_0)]} \tag{3}$$

Therefore, with the knowledge of the ratio of populations in the first two vibrational levels and the quenching to vibrational transfer ratio out of $v' = 1$, the temperature can be determined. A significant advantage to this method is that only the relative vibrational populations are needed. Thus, since THAF uses a single laser source, this negates the need to account for laser sheet intensity variations. In the present study, an image splitting arrangement was used to capture the two fluorescence images using a single camera, thereby reducing the need for optical calibration as well. This can be shown by considering the equation for the fluorescence collected from a given transition (n–m) [20]:

$$F_{nm} = \eta\varepsilon V_f \frac{\Omega}{4\pi} A_{nm} N_n \tag{4}$$

Since both fluorescence signals are collected on a shot-by-shot basis using the same laser and camera setup, the light

collection efficiency ε, the quantum efficiency η, laser focal volume V_f and the solid collection angle Ω need not be known explicitly. Thus by substituting Eq. (4) into the population ratio in Eq. (3), the temperature can be expressed in terms of the measured fluorescence:

$$T = \frac{-\Delta E_{10}/k}{\ln\left[\left(1+\frac{Q_1}{V_{10}}\right)\cdot\left(\frac{F_{1j}}{F_{0i}}\right)\cdot\left(\frac{A_{0i}}{A_{1j}}\right)\right]} \quad (5)$$

where F_{0i} and F_{1j} are the fluorescence signals from the first two levels of the $A^2\Sigma$ excited state to levels i and j of the $X^2\Pi$ ground state. There are a limited number of vibrational transitions that are practical to furnish the fluorescence ratio in Eq. (5). The fluorescence from the (1–0) vibrational band is the optimal choice to measure the population of $v' = 1$ since it is the most intense transition from this level and is well removed from the pump wavelength, thereby eliminating any interference issues. For the population of $v' = 0$, the (0–0) band is an excellent option since it is the strongest vibrational transition of OH. However, in highly particulate environments, scattering interferences of the laser pump wavelength can overcome the fluorescence from this band. In addition, the (0–0) band has a greater susceptibility for self-absorption. One alternative is to use the fluorescence from the (0–1) vibrational band. Unfortunately, this band is significantly weaker than the (0–0) band, which is an important consideration for two-dimensional measurements where fluorescence intensity is at a premium.

The population ratio was obtained by optically integrating the fluorescence from the selected vibrational bands and using the corresponding spontaneous emission coefficients A_{0i} and A_{1j} tabulated by Luque and Crosley [21]. However, due to the broadband collection approach that was employed, there are other OH vibrational bands that will interfere with the fluorescence signal from the desired transition. The (0–0) and (1–0) vibrational bands are overlapped primarily by the (1–1) and (2–1) vibrational bands respectively. To subtract the contribution of these unwanted bands based on the intensity of each pixel, the iterative method proposed by Joklik [18] was employed. This method is most simply explained in a three-step process:

1. The magnitude of the (1–1) contribution to the (0–0) band is estimated using the (1–0) fluorescence signal. Since the (1–1) and (1–0) bands originate from the same level, simple algebraic manipulation of Eq. (4) yields an expression of the (1–1) fluorescence in terms of the (1–0) fluorescence:

$$F_{11} = A_{11}(F_{10}/A_{10}) \quad (6)$$

   This initially assumes no contribution of the (2–1) band.
2. The magnitude of the (2–1) fluorescence intensity is estimated by applying a population balance to the $v' = 2$ level similar to the derivation of Eq. (3):

$$T = \frac{-\Delta E_{21}/k}{\ln[(1+Q_2/V_{21})N_2/N_1]} \quad (7)$$

$$F_{21} = F_{11}\left(\frac{A_{11}}{A_{21}}\right)\frac{\exp(-\Delta E_{21}/kT)}{(1+Q_2/V_{21})} \quad (8)$$

   An initial temperature must be assumed at the start of the iteration, and the values of Q_2/V_{21} and Q_1/V_{10} are assumed equal.
3. The fluorescence estimates of the (2–1) and (1–1) are subtracted from the (1–0) and (0–0) respectively, and a temperature is calculated from Eq. (5). The process is repeated until the temperature converges.

The validity of detailed balancing applied to vibrational levels via Eq. (2) is cause for some debate [16,17]. A constant vibrational energy transfer rate V_{nm} and energy spacing ΔE_{nm} assumes that the significance of the rotational energy level interaction within each vibrational level is small. The value of V_{nm} will therefore represent the averaged rate of transfer between the rotational manifolds contained in vibrational states n and m. However, the distribution of molecules within the rotational manifold is not constant with changes to the laser populated rotational level. Although the rotational redistribution within the $v' = 0$ level will reach an equilibrium shortly into the laser pulse, it has been shown by Zizak et al. [15] that the influence of laser pumping produces an over-population in rotational states near the laser populated level with respect to a Boltzmann distribution. Thus it seems intuitive that if a higher rotational level is populated by the laser, the overall distribution among rotational states will be more energetic, thereby producing a greater propensity for upward vibrational energy transfer to the $v' = 1$ level. If this is the case, the population ratio N_1/N_0 that results from the vibrational energy transfer will not only depend on the temperature, but also on the rotational transition that is targeted by the excitation laser. This issue is re-examined in the current work by pumping different rotational lines and comparing the difference in the vibration population ratio.

The ratio of quenching to vibrational transfer Q_1/V_{10} is another important consideration to this theoretical treatment since this value must be obtained before an accurate temperature can be calculated. As indicated briefly in the introduction, there are two approaches to calculating these collisional transfer rates. An analytical approach requires knowledge of quenching and VET cross sections, relative velocity (temperature), and the number density of colliding species. Collisional cross section information is available from a number of different sources [18,22–26] and species concentrations can be estimated for a set of conditions through a numerical combustion code. The results of such an analytical treatment in a $C_2H_2/O_2/N_2$ flame presented by Joklik [18] indicate that Q_1/V_{10} is slightly temperature dependent, thus producing an approximately linear rise in values from 0.5 to 0.6 in the 1600 to 2600 K temperature range. The second approach is to account for this term

through calibration at a known temperature value. Considering the effort and uncertainties associated with calculating these rates analytically, this experimental method is quite straightforward. By measuring the fluorescence ratio at a location where temperature is a known quantity, the quenching to vibrational transfer ratio can be calculated by re-arranging Eq. (5). It is important to use reliable temperature calibration data since the accuracy of subsequent THAF measurements are dependent on this calibration. Sodium line reversal measurements in a reference flame studied by Lewis and von Elbe [27] were therefore used in the present work to calibrate the images via the Q_1/V_{10} term. Since the quenching and VET rates vary with species concentrations, temperature, and rotational energy, the range of applicability of a single calibration was assessed for conditions tested in this work. If the Q_1/V_{10} ratio is sensitive to variations of one or more of these conditions, these properties must be held constant between the calibration flame and the desired measurements.

3. Experimental setup

The general experimental setup for obtaining 2-D fluorescence data at two separate wavelengths using a single laser source and an intensified CCD camera is shown in Fig. 3. The laser light was produced by a Lumonics Nd:YAG pumped dye laser circulating Rhodamine 640 dye in methanol. A frequency doubling crystal reduced the wavelength to approximately 308 nm needed to excite a rotational line of OH from the ground $v'' = 0$ $X^2\Pi$ state to the $v' = 0$ level of the $A^2\Sigma$ excited state. Vibrational energy transfer then populated the higher energy levels, and the resulting fluorescence was passed through a Princeton Instruments beam-splitter to separate the desired vibrational bands. To circumvent the high signal losses of band-pass filters, dichroic beam splitters were used to separate the vibrational bands of interest. Dichroic coatings transmit or reflect, depending on the incident wavelength. In effect, they acted as both a beam splitter as well as a high efficiency filter. In order to discriminate between the (1–0) and (0–0) vibrational bands at 282 nm and 308 nm respectively, the transition from reflection to transmission needed to be quite steep, and centered at 295–300 nm. Since the (0–1) band was also to be tested in place of the (0–0) band, the dichroic would also have to transmit up to 360 nm. The dichroic that best suited these requirements was a Chroma model Q298lp with a transmission curve as shown in Fig. 4. The isolation of the (0–1) vibrational band required the addition of a 10 nm band-pass filter centered at 345 nm.

The two fluorescence images were incident on a 576 × 384 pixel Princeton Instruments intensified CCD camera fitted with a Nikor f/4.5 105 mm UV lens. Thermo-electric cooling minimized dark current noise. Camera control was achieved via a Princeton Instruments FG-100 pulse generator and ST-130 detector–controller, and the images were recorded using WinView camera software on a PC. Post-processing of the fluorescence images was done by a numerical code, which iteratively subtracted the unwanted vibrational bands and converged to a temperature value on a pixel-by-pixel basis to create the final temperature image.

The flame was produced from a rectangular shaped Bunsen burner fueled by natural gas premixed with air. Air-to-fuel ratios were adjusted by means of two rotameters. The rectangular burner was constructed to the specifications outlined by Lewis and von Elbe [27] with the intent to reproduce the flames in their work and thus make use of the sodium line reversal temperature contours for calibration and comparative purposes. The dimensions of the inner rectangular cross section were approximately 6.4 mm × 22.2 mm (1/4 in. × 7/8 in.) with a mixing length of about 1 m to provide a steady flame. To reduce the influence of drafts on the flame, a shield was constructed from acrylic sheeting which was designed to fit around the burner.

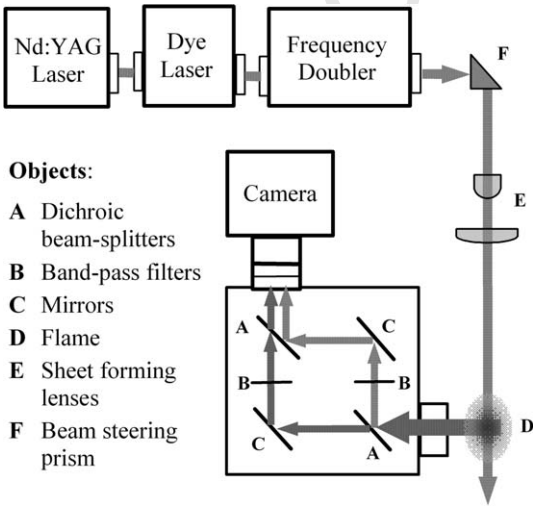

Fig. 3. Experimental setup.

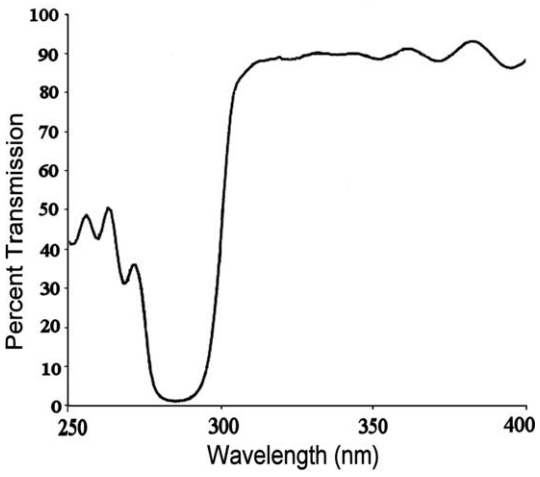

Fig. 4. Transmissivity of the dichroic beam splitter.

4. Results and discussion

4.1. Image processing

With the dye laser tuned to the $Q_1(6)$ rotational transition of the (0–0) vibrational band at 32380.99 cm^{-1} [28], the 5 cm high sheet of laser light produced two fluorescence images on the 576×384 camera viewing area as shown on the left of Fig. 5. The alignment of these two images was performed prior to the experiment by setting up a cross-hair target in front of the camera and adjusting the angle of the mirrors in the wavelength splitting arrangement shown in Fig. 3. It was estimated that the corresponding pixels used to calculate the fluorescence ratio were matched within one or two pixels.

Before the ratio was calculated, a number of image processing steps were taken to improve the fluorescence signal, remove background noise, and reduce data scatter. Most signal processing was applied to the fluorescence images before any temperature calculations were made. The following image processing steps were performed for each temperature image: multiple shot (accumulative) averaging, background subtraction, pixel smoothing, and overlapping band subtraction. The first step, accumulated averaging, was facilitated by the camera control software, which produced a final image from the summation of multiple exposures. The ratio of the two accumulated fluorescence images was therefore a numerical frame average over the number of images selected by the user. Frame averaging sacrifices instantaneous information but was necessary due to the low fluorescence signal strengths.

The second step was to subtract the background noise from the raw fluorescence image. The largest contributor to background noise is the signal generated by the detector when there is no incident radiant energy, commonly termed dark current. To account for dark current, a separate accumulated image was recorded with the lens cap on and subtracted from the raw fluorescence data on a pixel-by-pixel basis. Care was taken to allow the thermoelectric cooler to reach steady state before collecting multiple shot data to insure a steady average dark current background. Other possible sources of non-fluorescence interference such as flame luminescence, Rayleigh scattering, and Mie scattering that could contribute to the signal as a result of the broad wavelength range collected using dichroic splitters also needed to be considered. In order to determine if these interferences were a concern, an accumulated image of the flame was captured with the laser tuned slightly off fluorescence. These non-fluorescence interferences contributed no more than one or two intensity counts per camera shot and were therefore ignored.

Following background subtraction, each image was post-processed with a pixel-smoothing algorithm which averaged each pixel with its neighbors. Pixel smoothing, or in some cases pixel binning where a group of pixels are combined, is quite common in low light image processing. It helps to reduce the random nature of the fluorescence signal, as well as the variation in pixel response. Beyond reducing data scatter, spatial averaging also helps to reduce the error in the fluorescence ratio that could result from an imprecise image alignment.

Finally, after processing the fluorescence images in this manner, the temperature calculation could be performed pixel-by-pixel. Since band-pass filters were not used to isolate the (0–0) and (1–0) vibrational bands, in order to remove the fluorescence of the unwanted (2–1) and (1–1) vibrational bands, the afore-mentioned iterative subtraction technique was employed, converging to a temperature value at each pixel. To test the (0–1) band in place of the (0–0) band, the band-pass filter was necessary despite a peak transmission of approximately 40%.

4.2. Results using the (0–0) and (1–0) vibrational bands

To substantiate the use of vibrational THAF of the OH radical for temperature imaging in a practical application, it was important to test the technique under a variety of flame conditions. This allows a sense of the range of applicability

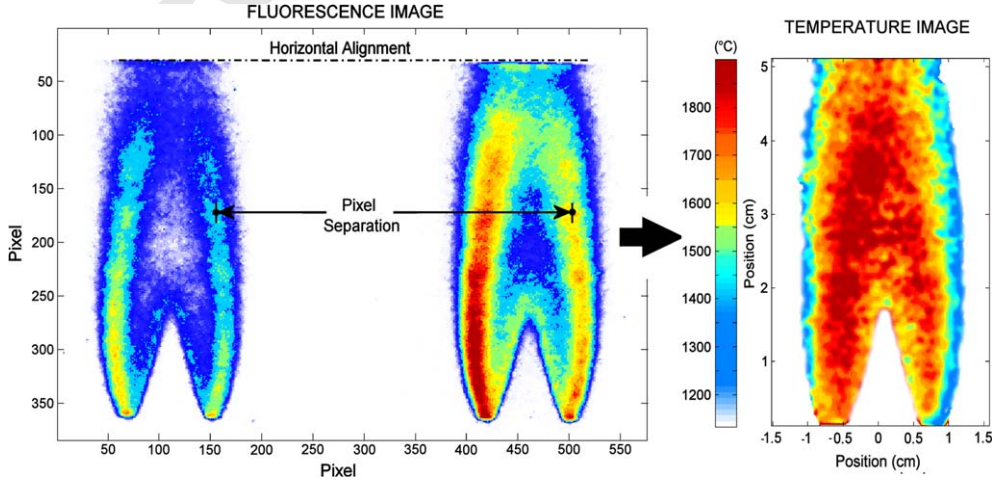

Fig. 5. Fluorescence images and the corresponding temperature field.

of a single Q_1/V_{10} calibration and the general accuracy that can be expected. Therefore, planar temperature measurements from three flames with equivalence ratios of 0.87, 1.03 and 1.33 were measured and are presented in Figs. 6–8 respectively. These three temperature maps are the result of applying the THAF technique to 500 shot accumulated fluorescence images of the (0–0) and (1–0) vibrational transitions. A colour map is used to indicate the temperature value in degrees Celsius.

In order to get a sense of the qualitative agreement between the thermally assisted fluorescence temperature images and the sodium line reversal data, isothermal lines that were produced by Lewis and von Elbe [27] were overlaid onto the THAF images. These temperature isotherm contours are the result of over 250 individual sodium line reversal temperature measurements in each of the three methane–air flames. The sodium line reversal technique is a well-established, non-intrusive optical technique for temperature measurements in reactive flows, and with careful calibration, it boasts a superb level of accuracy. The rectangular burner used in the current experimental investigation was constructed to the specifications published in Ref. [27] with the intent to reproduce these flames and use the temperature contours for calibration and comparative purposes. Temperature profiles from both methods at different levels above the burner are also compared on the right of Figs. 6–8. Since the pixel averaging serves to mask the data scatter, the standard deviation of a five by five pixel grouping was calculated prior to this step. Error bars representing two standard deviations of this pixel grouping are included periodically across the temperature profiles for reference. While this value does not strictly represent the uncertainty of the THAF measurement, it does give some insight into the distribution of random error.

The four works dealing with vibrational OH thermally assisted fluorescence [16–18,29] indicate an expected accuracy of single-point temperature measurements between 50 and 100 K. Recognizing that temperature imaging is more susceptible to a range of inaccuracies inherent with two-dimensional signal collection, the level of agreement that was achieved between the (0–0) (1–0) THAF temperature images and sodium line reversal images is very encouraging. Fig. 9 gives a graphical representation of the agreement between the current results and those published by Lewis and von Elbe [27] by plotting point temperature data from each method against the other. In this figure, three lines are included for reference, the middle representing perfect agreement, and the two dashed lines showing ±100 °C error bounds. Most of the data from the current investigation is easily within ±100 °C of sodium line reversal temperatures. For each flame, Table 1 lists the root mean square (RMS) deviation between the two measurement techniques calculated from a number of point temperature values taken from the profiles in Figs. 6–8. The best agreement was achieved in the lean and stoichiometric flames on account of the stronger signal resulting from a greater OH concentration under these conditions.

4.3. Quenching to vibrational transfer ratio

The dichroic filters reflect and transmit with different efficiencies and will therefore introduce a slight optical bias to the detected fluorescence signal. This bias will be even more pronounced when detecting the (0–1) vibrational

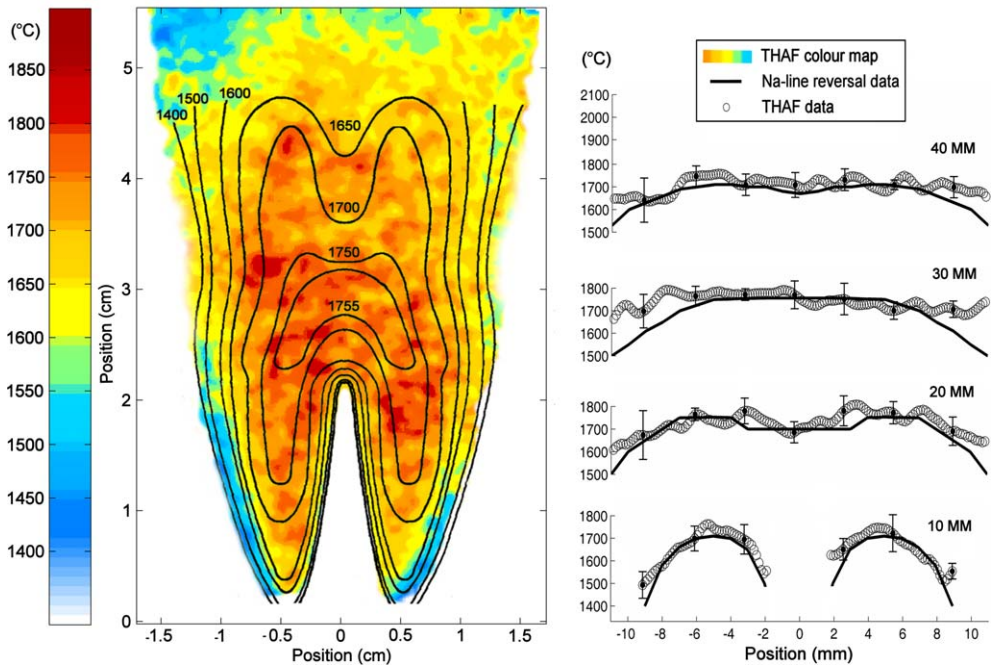

Fig. 6. Left: (0–0), (1–0) THAF temperature map with Na-line reversal isotherms; Right: temperature profile comparison ($\phi = 0.87$).

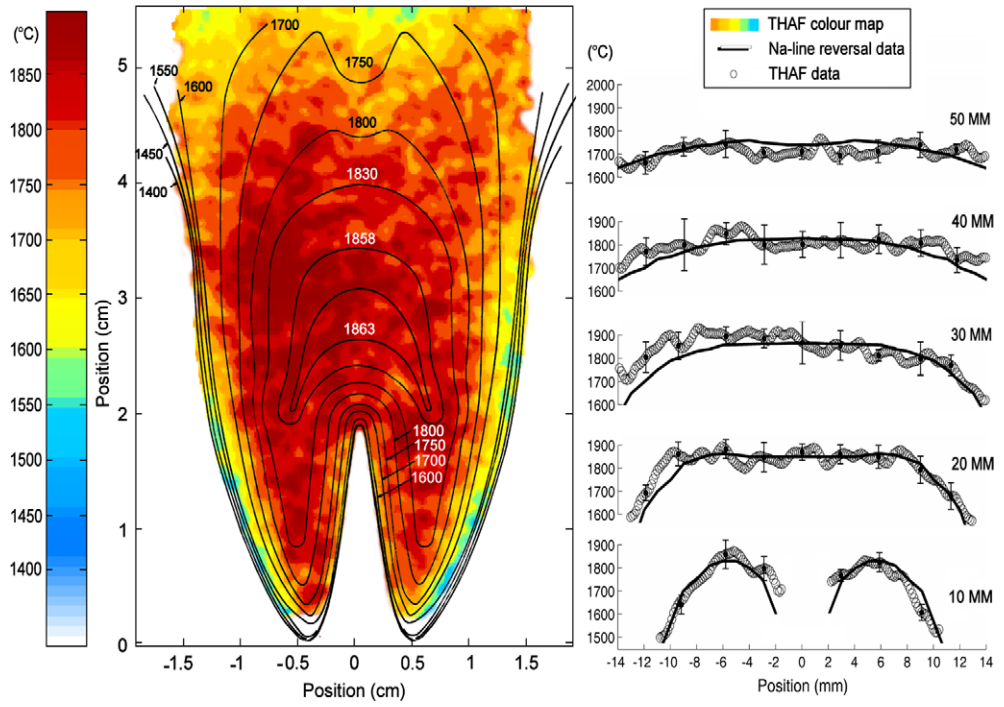

Fig. 7. Left: (0–0), (1–0) THAF temperature map with Na-line reversal isotherms; Right: temperature profile comparison ($\phi = 1.03$).

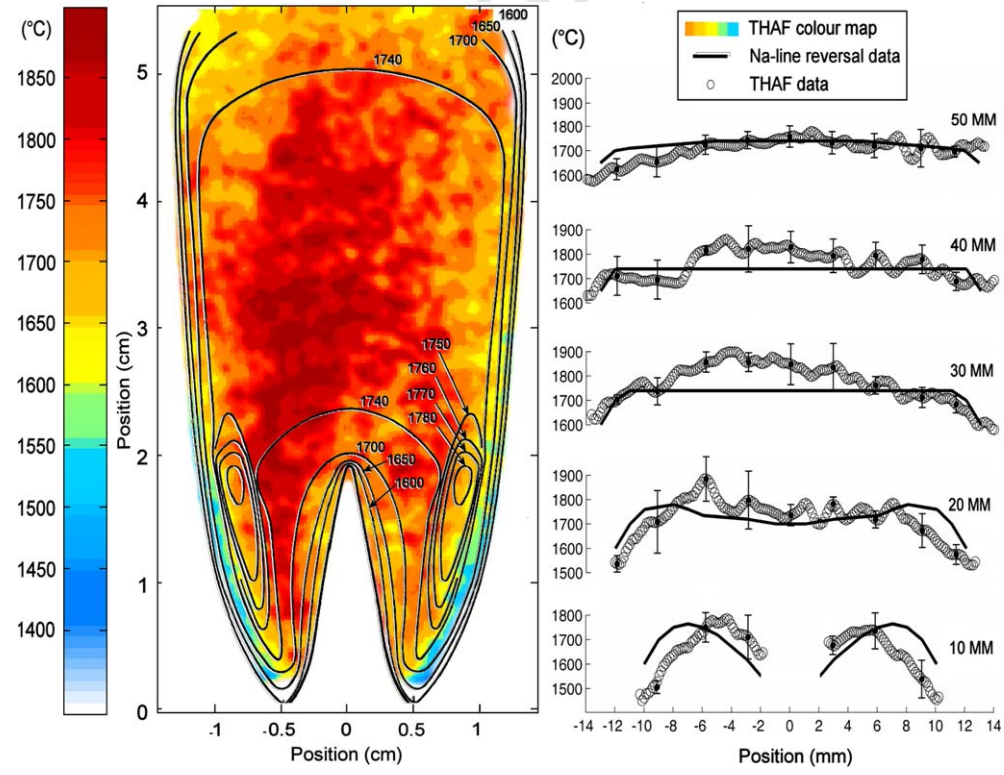

Fig. 8. Left: (0–0), (1–0) THAF temperature map with Na-line reversal isotherms; Right: temperature profile comparison ($\phi = 1.33$).

band since the band isolation filter will attenuate this signal approximately 50% more than the (1–0) band. However, since this bias is essentially constant, it is easily accounted for through a single calibration. Following the treatment of Dyer and Crosley [17], if the optical bias is included with the Q_1/V_{10} calibration, this produces an "effective"

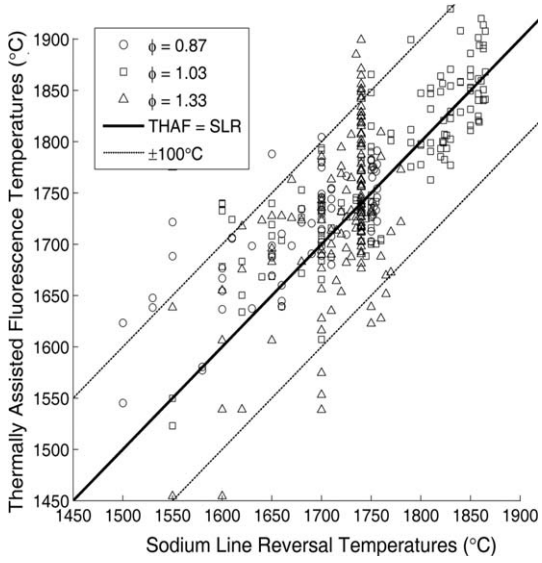

Fig. 9. Sodium line reversal and thermally assisted temperature comparison.

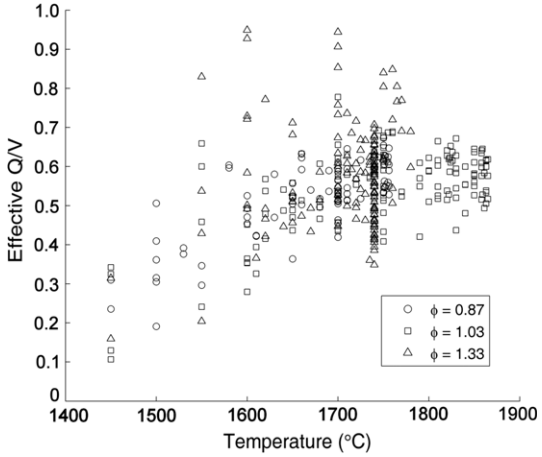

Fig. 10. Effective quenching to vibrational transfer ratio versus temperature.

Q_1/V_{10} value which is simply calculated by rearranging Eq. (5) and substituting the fluorescence ratio measured at a location with a known temperature value:

$$\left(\frac{Q_1}{V_{10}}\right)_{\text{eff}} = \frac{\exp(-\Delta E_{10}/kT)}{(F_{1_j}/F_{0i})\cdot(A_{0i}/A_{1j})} - 1 \tag{9}$$

Accurately accounting for the Q_1/V_{10} term under different conditions was of some concern, as the work by Joklik [18] indicated a more complex solution than a simple single-point calibration. Due to the temperature dependency of the quenching and VET rates, he elected to use a temperature dependent calibration term that reflected his experimental results. In addition, since the concentration of collider molecules shapes the quenching dynamics of the OH radical, the Q_1/V_{10} term will be dependent on the mixture fraction as well. Therefore, it was encouraging to discover that a single effective calibration value of 0.59 was sufficient to produce accurate results under the experimental conditions presented here.

To ascertain the behavior of the Q_1/V_{10} term with changes in temperature, the sodium line reversal data from the temperature profiles in Figs. 6–8 was substituted into Eq. (9), along with the measured fluorescence ratio at each corresponding pixel. This yielded the value of the calibration term for various flame temperatures as shown in Fig. 10. This plot suggests that the quenching to vibrational transfer ratio is indeed moderately dependent on the temperature, as first suggested by Joklik [18]. Thus, although a single calibration was used with good success in the current work, a temperature dependent calibration may be necessary when measuring a broader range of flame temperatures.

4.4. Laser pumping effects

As outlined in the theoretical discussion, there is some question as to the applicability of a single transfer rate to describe the energy exchange between the upper state vibrational energy levels. Crosley and Smith [16] first raised a question as to the validity of using detailed balancing to describe vibrational energy transfer via Eq. (2). Despite this uncertainty, their experimental results did not indicate any significant variation in the upper state vibrational population ratio N_1/N_0 for different rotational pump lines. However, Dyer and Crosley [17] re-examined the issue and found that for three selected laser-populated rotational levels, there was a smooth increase in the population ratio. To resolve these conflicting results, the laser was separately tuned to six different rotational Q-branches of the (0–0) vibrational band. The population ratio was calculated from the resulting fluorescence and plotted in Fig. 11 against the energy of each rotational level. These results confirm the work of Dyer and Crosley [17] by showing a general trend of rising vibrational population ratios with the increase in rotational energy of the laser pump level. While this result was anticipated, it does introduce a question as to the validity of the THAF theory for deriving temperature from

Table 1
Experimental specifics for each of the thermally assisted fluorescence images

Figure	Air flow $\left(\frac{\text{cm}^3}{\text{s}}\right)$	CH_4 flow $\left(\frac{\text{cm}^3}{\text{s}}\right)$	Equivalence ratio (ϕ)	Detection scheme	Number of camera shots	RMS error $\sqrt{\frac{\Sigma(\text{THAF}-\text{SLR})^2}{n}}$
6	195	18	0.87	(0–0), (1–0)	500	52.1 °C ($n = 77$)
7	200	22	1.03	(0–0), (1–0)	500	44.0 °C ($n = 130$)
8	140	19.5	1.33	(0–0), (1–0)	500	66.7 °C ($n = 129$)
12	195	18	0.87	(0–1), (1–0)	500	70.6 °C ($n = 77$)

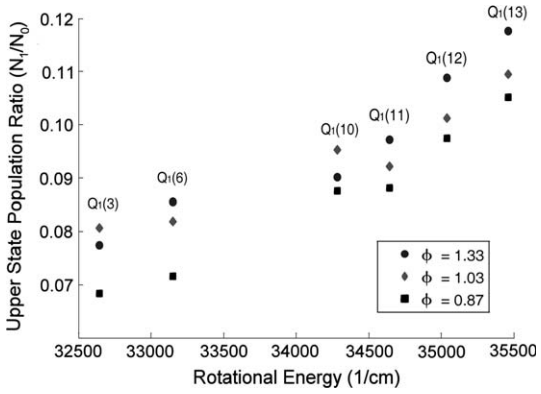

Fig. 11. Changes in vibrational energy state population ratio with different laser pump lines.

vibrational energy transfer. To some degree, this issue is a matter of perception. From the perspective of an engineering experimentalist, while the use of detailed balancing to describe vibrational energy transfer might be somewhat questionable, as long as the same rotational line is used for both calibration and experimentation, the derived THAF theory will hold.

4.5. Substituting the (0–1) for the (0–0) band

The results presented thus far have made use of the (0–0) band to furnish the population of the $v' = 0$ vibrational level. The inherent intensity of this band is simultaneously the source of commendation and criticism. A strong signal reduces random error but also can introduce systematic error due to a propensity for self-absorption as the signal passes through the combustion medium. In addition, to avoid scattered interference, it is advantageous to be able to collect fluorescence at a wavelength that is distinct from the laser excited transition. Thus, the (0–1) band located at 346 nm was ostensibly an attractive option. However, the price of reduced laser interference is significantly lower signal levels. The average (0–1) fluorescence per camera shot was typically no more than a few counts above the background signal. This made it a delicate task to separate the fluorescence from signal noise. Despite these difficulties, temperature imaging was attempted using the (0–1) (1–0) fluorescence pair. The use of the (0–1) band isolation filter required a different effective calibration value than that of previous results. A 500 shot temperature image of the lean ($\phi = 0.87$) flame using this detection scheme is shown in Fig. 12. The temperature profiles on the right of this figure still follow the sodium line reversal data with a fair degree of accuracy, albeit with larger random error. This does demonstrate that the THAF theory holds true for the (0–1) band, but the weakness of the signal makes any regular use of this band very restrictive. Once the fluorescence signal drops to such a low value, sensitivity to small inaccuracies in calibration or signal processing make accurate results very difficult to achieve on a consistent basis.

5. Uncertainty analysis

The use of the hydroxyl radical for temperature imaging has some inherent limitations. Since the concentration of OH molecules drops off rapidly below approximately

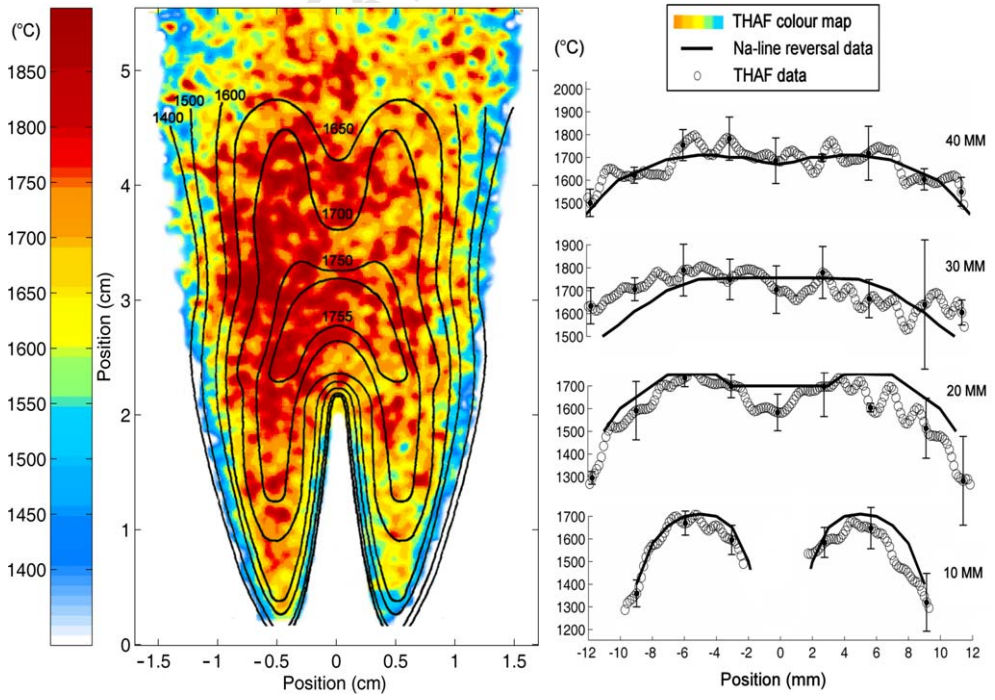

Fig. 12. Left: (0–1), (1–0) THAF temperature map with Na-line reversal isotherms; Right: temperature profiles ($\phi = 0.87$).

1500 K, this produces low fluorescence signals in cooler regions of the flame. An oxygen-enriched flame typical of those used in other publications [17,18] would have significantly increased the fluorescence signal due both to the increase in temperature and the available oxygen for OH formation. The accuracy of the method also suffers in areas of rich or extremely lean fuel mixtures due to the reduced OH concentration under these conditions. This can be demonstrated by comparing the signal to noise ratio (SNR) of the fluorescence signal from each of the three fuel mixtures. To estimate the value of the single shot SNR, twenty single-shot fluorescence images of each flame were collected using 288×192 pixel resolution (2×2 binning). The signal to noise ratio of each pixel could then be calculated by dividing the numerical mean by the standard deviation. This calculation includes shot noise and any random fluctuation in the fluorescence signal due to the unsteady reacting flow. The result of such a calculation for each pixel is provided in Fig. 13 and demonstrates the decline in the signal to noise ratio of the (0–0) vibrational band under rich conditions. Thus, the best temperature agreement was achieved in stoichiometric or slightly lean flames where the temperature is highest and the mixture is conducive to higher OH production.

Perhaps more significant, however, are the limitations of the vibrational thermally assisted method itself. Due to the reliance on vibrational energy transfer to populate the upper vibrational manifold, the fluorescence from these levels will be limited by the efficiency with which this process occurs. Considering the temperature range of a methane–air flame, no more than ~10% of OH molecules are collisionally excited from $v' = 0$ to $v' = 1$ (Fig. 11). Referring to Eq. (4), the intensity of the fluorescence signal from a given band is dependent on the population density of the excited level and the propensity for spontaneous emission (A_{ij}). Since Einstein's coefficient for spontaneous emission decreases with increasing vibrational level, the magnitude of the fluorescence from the (1–0) vibrational band is merely 2–3% that of the (0–0) vibrational level. This is in large part attributable to the large energy spacing ($\Delta E_{10} = 3000\ \mathrm{cm}^{-1}$) between the first two vibrational energy levels of OH. The larger the energy spacing, the less vibrational energy transfer, and therefore the greater the propensity for measurement uncertainty resulting from a noisy signal. This is clearly seen in Fig. 14 where the SNR in the lean flame is calculated for each of the vibrational bands from 20 single-shot measurements similar to Fig. 13. The fluorescence SNR drops from approximately 4 in the (0–0) image to approximately 1.5 in the (1–0) image. The extremely low SNR in the (0–1) fluorescence image is the result of a low spontaneous emission constant A_{01}.

Despite the increase in signal noise, a large energy gap between fluorescence levels is also beneficial as it indicates that any random error in the measurement of the fluorescence ratio will result in smaller errors in the temperature calculation. This can be demonstrated by expressing Eq. (5) in a differential form as follows:

$$\frac{\mathrm{d}(F_{1j}/F_{0i})}{F_{1j}/F_{0i}} = \frac{\Delta E_{10}}{kT} \cdot \frac{\mathrm{d}T}{T} \tag{10}$$

The differential on the left of Eq. (10) is essentially the noise associated with the fluorescence ratio. This is typically related to the signal to noise ratio of the two fluorescent bands as follows [8]:

$$\frac{\mathrm{d}(F_{1j}/F_{0i})}{F_{1j}/F_{0i}} = \frac{1}{\mathrm{SNR}_R} \approx (\mathrm{SNR}_{0i}^{-2} + \mathrm{SNR}_{1j}^{-2})^{1/2} \tag{11}$$

The term $\Delta E_{10}/kT$ in Eq. (10) is referred to as the slope sensitivity, as it determines the sensitivity of the temperature calculation to the signal noise. By collecting fluorescence from the first two vibrational levels of the OH radical at 2000 K, the relatively large slope sensitivity will reduce a

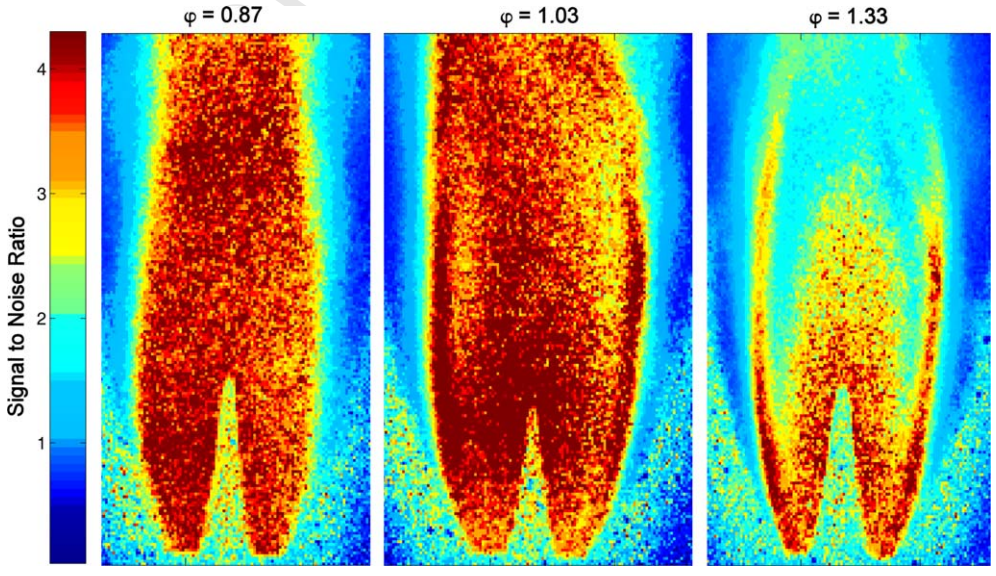

Fig. 13. The (0–0) fluorescence signal to noise ratio in each of the three flames.

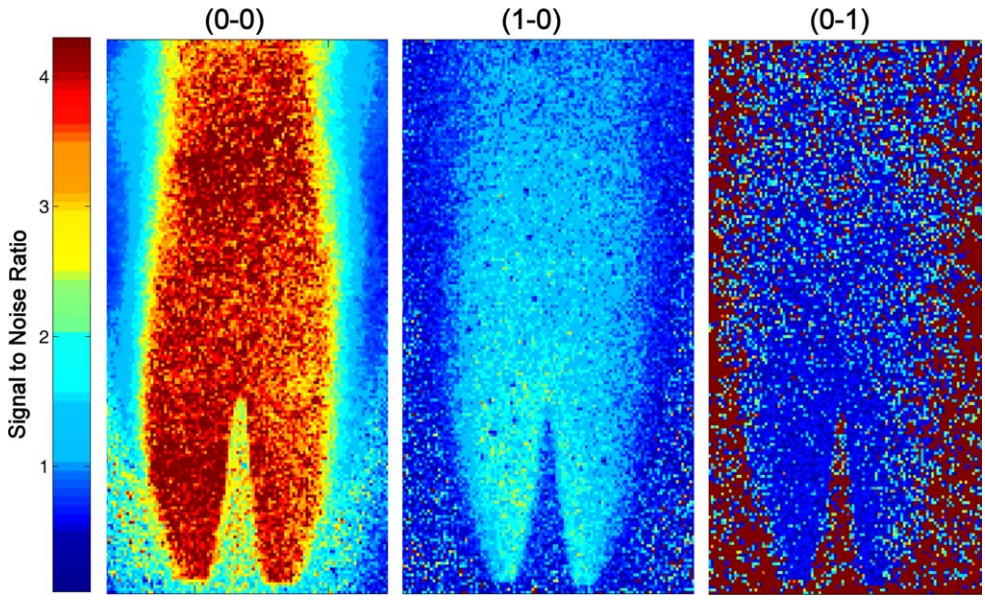

Fig. 14. Fluorescence signal to noise ratio in the lean ($\phi = 0.87$) flame resulting from the (0–0), (1–0) and (0–1) vibrational transitions.

10% error in the fluorescence ratio to a 5% error in the temperature measurement. A number of authors dealing with the two-line measurement technique [7–10] have sought to find a suitable tradeoff by selecting two rotational transitions that are sufficiently separated for good measurement sensitivity, but not at the expense of an ample fluorescence signal. While this is commonly achieved by selecting an energy spacing $\Delta E_{10} \approx kT$, Seitzman and Hanson [8] comment that due to the non-linear relationship between temperature and the fluorescence ratio, it is advantageous to select a larger energy spacing for images with a lower SNR. Otherwise, the measurements on the edges of the fluorescence noise distribution resulting from multiple shots will have an undesirably large impact on the temperature calculation. This results in a multiple-shot averaged temperature value that is skewed from the true mean temperature. However, in the present circumstances, the energy spacing associated with vibrational THAF of the OH molecule is likely too large for temperature measurements below 2000 K, essentially limiting this technique to multiple shot imaging under these conditions. An increase in the measured temperature should greatly improve the available signal. First, it would increase the overall OH concentration, and second, increase the rate of VET, thereby strengthening the weaker (1–0) fluorescence. Thus in a higher temperature range, single shot imaging might prove feasible using this method, especially if a high powered tunable laser is used.

Apart from flow and mixture fluctuations, the primary source of random experimental uncertainty is photon shot noise. Shot noise is the natural outcome of the random photon flux incident on to the optical detector. The statistical distribution of shot noise follows a Poisson distribution, which possesses a square root relationship with the signal. Therefore, a multiple exposure fluorescence image should increase the SNR by a factor equal to the square root of the number of exposures. Considering a 500 shot average of the fluorescence signal, the signal to noise ratio of the fluorescence ratio (SNR_R) can be estimated from Eq. (11) by using the single shot SNR values in Fig. 14 multiplied by a factor of $\sqrt{500}$. For the (0–0) (1–0) fluorescence pair, this produces a SNR_R equal to ~26 (4% error) resulting in a 2% (40 K) temperature uncertainty. A similar calculation for the (0–1), (1–0) fluorescence pair produces a 3.7% (75 K) temperature uncertainty. This compares well with the values for the RMS deviation between the THAF and SLR temperatures provided in Table 1.

Another issue associated with the current experimental approach is the strong propensity for radiation from the (0–0) vibrational band to be absorbed as it propagates through the combustion medium containing OH radicals. This introduces two separate but related effects. First, since the laser was tuned to this transition, the energy of the laser sheet was reduced by 20–30% across the flame width. The amount of laser absorption depends on the density distribution of absorbing OH molecules and the rotational pump line that is selected. This laser attenuation should not have any affect on the temperature measurement since the fluorescence ratio at a given point from molecules excited by the same laser is theoretically invariant with changes in laser intensity. However, since the reduced laser power will promote less OH as it propagates from left to right, this will produce a weakening fluorescence signal and an increase in shot noise in this direction. Referring to Figs. 13 and 14, there is a noticeable decrease in the signal to noise ratio from left to right. An increase in the oscillation of the temperature profile in this direction is also perceptible on the right of Fig. 12. The low (0–1) fluorescence signal in this figure accentuates the effect of lower laser energy on the degree of measurement uncertainty.

Self-absorption (radiation trapping) of the fluorescence signal is the second observable consequence of the strong absorption characteristics of the (0–0) band. Since the fluorescence source is located at some distance from the point of observation, the radiation signal is absorbed by the OH molecules along this path. Following self-absorption, the quantity of fluorescence being measured will no longer represent the fluorescence produced at the plane of laser excitation from which the theory is derived. Since the amount of self-absorption is directly related to the strength of the transition that is being measured, the most common method to avoid self-absorption is to select a transition with a low inherent absorption propensity. Naturally there is a trade-off between the signal strength and optical depth. From the laser absorption measurements, a value of 10–15% was estimated for the self-absorption of the (0–0) fluorescence signal. A similar result for this band is given by Joklik [18], along with a measured value of 3.5% for the trapping of the (1–0) band.

Since the (0–0) band is preferentially self-absorbed by the combustion medium, this will introduce a bias into the fluorescence ratio that could cause a temperature error. This bias is largely accounted for through the effective calibration relating the fluorescence ratio to a known temperature. However, since radiation trapping is a function of the number of absorbing molecules along the path length, this will change from pixel to pixel, as will the required calibration. To get a sense of the systematic error that could result from a single calibration approach, consider two points where the path length of the first is half that of the second point (or equally, half the number of absorber molecules). This will result in a 4% change in the fluorescence ratio as a result of the difference in self-absorption. Thus, if the first point was used for the temperature calibration, the second point would contain an error of ~40 K due to self-absorption. This example illustrates that while self-absorption is an important consideration, the systematic errors that result from a calibrated THAF measurement are unlikely to be a significant deterrent. One very useful method for reducing the influence of trapping is to select a plane of laser excitation in the edge of the combustion zone nearest to the camera. This reduces the absorptive path that the signal must travel and therefore the amount of self-absorption.

Systematic errors associated with the experimental equipment mainly arise from non-uniformities in the camera response. First, there are pixel-to-pixel irregularities, which lead to systematic measurement error. If a pixel collecting the (0–0) fluorescence is more sensitive to radiation than the corresponding pixel collecting the (1–0) fluorescence, the resulting discrepancy in the fluorescence ratio will produce a temperature bias. Pixel to pixel non-uniformity resulting from the image intensifier can be as high as 12% [5]. Therefore, spatial averaging of neighboring pixels was employed to reduce the influence of pixel irregularities. Even after spatial averaging, it was noted that repeated measurements with the same flame and camera settings produced similar irregularities in each temperature image. The repeatability of these irregularities pointed to camera response as the source of this error.

Another possible source of systematic error is the non-linearity in detector response. Once the fluorescence reaches the camera, it is generally assumed that the detector responds linearly to the incident fluorescence intensity. According to the camera manufacturer, the detector response linearity is better than 1% for the upper 95% of the intensity range but the lower 5% is reportedly slightly non-linear. Since the fluorescence resulting from the (1–0) and (0–1) vibrational bands is typically quite weak, there is a possibility that the camera response will be non-linear in these images. Consequently, if the intensified detector bit count is proportional to the fluorescence intensity across the (0–0) fluorescence image but exhibits a non-linear response to the corresponding (1–0) fluorescence, the fluorescence ratio will indirectly depend on laser power and could introduce a temperature bias with increased attenuation across the flame width. Although the flame temperature is noticeably asymmetrical about the axis of the burner, it is unclear if the non-linearity in camera response is the only cause.

Most other sources of systematic errors are accounted for by the calibration at a known temperature. The single-point calibration reduces systematic error by fixing the temperature at a single point. All other points then rely on the accuracy of the THAF theory and equipment reliability for a correct measurement. Of course, the accuracy of the calibration is dependent on the accuracy of the reference temperature measurement and on the ability to reproduce the reference flames. The sodium line reversal technique itself has a solid reputation for producing accurate results. Lewis and von Elbe [27] indicate a repeatability of 4 °C for the SLR results used in the present case. Joklik [18] indicates a more conservative uncertainty estimate of better than 20 K for the SLR calibration in his work. However, larger errors can be expected from any failure to match the flame conditions described in Lewis and von Elbe [27]. Although an effort was made to reproduce the flames as accurately as possible, small differences in flow conditions, fuel composition and burner construction would lead to some systematic calibration error.

6. Conclusions

This work has successfully applied thermally assisted fluorescence of the OH radical to temperature imaging in a methane–air flame. Using a single laser source in conjunction with a single intensified CCD camera, broadband fluorescence intensity measurements were collected from two vibrational bands. The resulting fluorescence images were post processed to produce a single temperature image. Agreement between these thermally assisted fluorescence images and sodium line reversal temperatures from a similar flame was generally better than ±100 °C. The main advantages to this technique are the relative simplicity of

the theory and experimental setup. By measuring a laser induced fluorescence ratio resulting from a single laser source, variations in the laser energy (pulse to pulse, as well as spatial variations) need not be accounted for. In addition, a single camera simplifies matters since there is no need to account for camera alignment and gain settings.

The second object of the current study was to get a sense of the range of conditions in which a single Q_1/V_{10} calibration would remain valid. This is important in the practical application of this technique. If the scope of a single calibration from a reference flame is quite limited, a separate calibration would be needed for each combustion environment. In this study, a single effective calibration value including Q_1/V_{10} produced satisfactory results in a temperature range between 1400 and 1900 °C. This calibration also showed little response to the difference in mixture fraction between the three premixed flames. This result is encouraging as it tends to indicate that the range of applicability of a single calibration is quite good. Thus, by using a calibration flame that is comparable to the experimental conditions being measured, accurate temperature images can be expected.

The use of a broadband filter centered at 345 nm to collect (0–1) fluorescence in place of (0–0) fluorescence was also tested as a feasible option. Although the results did follow the known temperature profile, the weakness of the signal made any regular use of this band extremely restrictive. Once the fluorescence dropped to a few counts per laser shot, accurate results were very difficult to achieve with any consistency. The signal from this band would improve with increased OH concentration and increased laser energy.

Despite the encouraging results in confirming the validity of the model and proving the applicability to temperature imaging, there are undoubtedly some areas that could be improved as well. The limiting factor in all the measurements was the level of available fluorescence. There are two principal explanations for the low signal intensity resulting from vibrational OH–THAF. The first is particular to the OH molecule and the conditions tested in the present work. Since OH production is highly dependent on the temperature and the mixture of the combustion medium, non-stoichiometric, low temperature regions produce concerns with low signal intensity. The second cause of a low signal is the limitation inherent to the vibrational THAF method itself. Due to the large energy spacing between vibrational energy levels, the measured temperature range must be reasonably high if a single-shot fluorescence signal is to be expected from the collisionally excited level. However, for averaged temperature measurements, this work has demonstrated that vibrational THAF provides an excellent alternative to comparable laser temperature techniques.

It is helpful to note that while the limitations that were encountered have been judiciously enumerated, most are common to thermometry methods that utilize fluorescence from the OH radical. Although there is certainly more freedom in the two-line technique to select suitable rotational transitions for the temperature range being measured, a balance between slope sensitivity and shot noise must be maintained. Seitzman et al. [7] present single shot images but note a shot-noise-limited random error of over 20%. Similarly, single shot two-line thermometry in an internal combustion engine yielded reasonably high uncertainties between 13% and 17% despite a high pressure environment well suited OH production [30]. Thus, even with the greater degree of experimental complexity typical of the two-line technique, it is still a challenge to achieve single shot temperature imaging due to the shot-noise limitations of a low OH fluorescence signal.

Acknowledgements

The financial support of the Natural Sciences and Engineering Council of Canada (NSERC) is gratefully acknowledged. The authors also thank Dr. E. Weckman for providing access to the LIF equipment.

References

[1] S. Kampmann, A. Leipertz, K. Dobbellin, J. Haumann, Th. Sattelmayer, Two-dimensional temperature measurements in a technical combustor with laser Rayleigh scattering, Applied Optics 32 (1993) 6167–6172.
[2] D. Most, A. Leipertz, Simultaneous two-dimensional flow velocity and gas temperature measurements by use of a combined particle image velocimetry and filtered Rayleigh scattering technique, Applied Optics 40 (2001) 5379–5387.
[3] R. Friedrich, A. Leipertz, Two-dimensional temperature determination in the exhaust region of a laminar flat-flame burner with linear Raman scattering, Applied Optics 36 (1997) 6989–6996.
[4] R.K. Mohammed, M.A. Tanoff, M.D. Smooke, A.M. Schaffer, M.B. Long, Computational and experimental study of a forced, time-varying, axisymmetric, laminar diffusion flameTwenty-Seventh International Symposium on Combustion, vol. 27, The Combustion Institute, 1998, pp. 693–702.
[5] J. Friedman, M. Renksizbulut, Investigating a methanol spray flame interacting with an annular air jet using phase-Doppler interferometry and planar laser induced fluorescence, Combustion and Flame 117 (1999) 661–684.
[6] B. Hiller, R.K. Hanson, Simultaneous planar measurements of velocity and pressure fields in gas flows using laser-induced fluorescence, Applied Optics 27 (1988) 33–48.
[7] J.M. Seitzman, R.K. Hanson, P.A. DeBarber, C.F. Hess, Application of quantitative two-line OH planar laser-induced fluorescence for temporally resolved planar thermometry in reacting flows, Applied Optics 33 (1994) 4000–4012.
[8] J.M. Seitzman, R.K. Hanson, Two-line planar fluorescence for temporally resolved temperature imaging in a reacting supersonic flow over a body, Applied Physics B 57 (1993) 385–391.
[9] B.K. McMillin, J.L. Palmer, R.K. Hanson, Temporally, resolved two-line fluorescence imaging of NO temperature in a transverse jet in a supersonic cross flow, Applied Optics 32 (1993) 7532–7545.
[10] M.P. Lee, B.K. McMillin, R.K. Hanson, Temperature measurement in gases by use of planar laser-induced fluorescence imaging of NO, Applied Optics 32 (1993) 5379–5396.
[11] G. Zizak, J.D. Winefordner, Application of thermally assisted atomic fluorescence technique to the temperature measurement in a gasoline-air flame, Combustion and Flame 44 (1982) 35–41.
[12] M.L. Elder, G. Zizak, D. Bolton, J.J. Horvath, J.D. Winefordner, Single pulse temperature measurements in flames by thermally assisted atomic fluorescence spectroscopy, Applied Spectroscopy 38 (1984) 113–118.

[13] R.G. Joklik, J.J. Horvath, H.G. Semerjian, Temperature measurements in flames using thermally assisted laser-induced fluorescence of Ga, Applied Optics 30 (1991) 1497–1504.
[14] C. Chan, J.W. Daily, Measurement of temperature in flames using laser induced fluorescence spectroscopy of OH, Applied Optics 19 (1980) 1963–1968.
[15] G. Zizak, J.J. Horvath, J.D. Winefordner, Flame temperature measurement by redistribution of rotational population in laser-excited fluorescence: an application to the OH radical in a methane–air flame, Applied Spectroscopy 35 (1981) 488–493.
[16] D.R. Crosley, G.P. Smith, Vibrational energy transfer in laser-excited $A^2\Sigma^+$ OH as a flame thermometer, Applied Optics 19 (1980) 517–520.
[17] M.J. Dyer, D.R. Crosley, Two-dimensional measurements of OH concentration and temperature in reactive flows, Report No: AFWAL-TR-84-2045, Air Force Wright Aeronautical Laboratories, Wright-Patterson Air Force Base, OH, 1984.
[18] R.G. Joklik, OH vibrational thermally-assisted laser induced fluorescence temperature measurements in flames, Combustion Science and Technology 87 (1991) 109–125.
[19] A. Burkert, W. Triebel, H. Stafast, Single shot imaging of gas temperatures in low temperature combustion based laser induced fluorescence of formaldehydeTwenty-Ninth International Symposium on Combustion, vol. 29, The Combustion Institute, 2002, pp. 1–13.
[20] R. Cattolica, OH rotational temperature from two-line laser-excited fluorescence, Applied Optics 20 (1991) 1156–1166.
[21] J. Luque, D.R. Crosley, Transition probabilities in the $A^2\Sigma^+$–$X^2\Pi$ electronic system of OH, Journal of Chemical Physics 109 (1998) 439–448.
[22] C.Y. Chan, R.J. O'Brlen, T.M. Hard, T.B. Cook, Laser-excited fluorescence of the hydroxyl radical: relaxation coefficients at atmospheric pressure, Journal of Physical Chemistry 87 (1983) 4966–4974.
[23] R.K. Lengel, D.R. Crosley, Energy transfer in $A^2\Sigma^+$ OH. II. Vibrational, Journal of Chemical Physics 68 (1978) 5309–5324.
[24] J. Burris, J.J. Butler, T.J. McGee, W.S. Heaps, Collisional deactivation rates for $A^2\Sigma^+$ $v' = 1$ state of OH, Journal of Chemical Physics 124 (1988) 251–258.
[25] K.L. Steffensa, D.R. Crosley, Vibrational energy transfer in OH $A^2\Sigma^+$ between 195 and 295 K, Journal of Chemical Physics 112 (2000) 9427–9432.
[26] M. Tamura, P.A. Berg, J.E. Harrington, G. Luque, J.B. Jeffries, G.P. Smith, D.R. Crosley, Collissional quenching of CH(A), OH(A), and NO(A) in low pressure hydrocarbon flames, Combustion and Flame 114 (1998) 502–514.
[27] B. Lewis, G. von Elbe, Stability and structure of burner flames, Journal of Chemical Physics 11 (1942) 75–97.
[28] G.H. Dieke, H.M. Crosswhite, The ultraviolet bands of OH, Journal of Quantum Spectroscopic Radiation Transfer 2 (1962) 97–199.
[29] A. A Neuber, J. Janicka, E.P. Hassel, Thermally assisted fluorescence of laser-excited OH $A_2\Sigma^+$ as a flame diagnostic tool, Applied Optics 35 (1996) 4033–4040.
[30] A. Cessou, U. Meier, D. Stepowski, Applications of planar laser induced fluorescence in turbulent reacting flows, Measurement Science Technology 11 (2000) 887–901.